OCCAM

OXFORD CENTRE FOR COLLABORATIVE APPLIED MATHEMATICS

Fractional diffusion models of cardiac electrical propagation : role of structural heterogeneity in dispersion of repolarization

by

Alfonso Bueno-Orovio
David Kay
Vicente Grau
Blanca Rodriguez
Kevin Burrage

OCCAM Preprint Number 13/35

Fractional diffusion models of cardiac electrical propagation: role of structural heterogeneity in dispersion of repolarization

Alfonso Bueno-Orovio[a],[1] David Kay,[2] Vicente Grau,[3] Blanca Rodriguez,[2] and Kevin Burrage[2,4]

[1] *Oxford Centre for Collaborative Applied Mathematics, University of Oxford, Oxford OX1 3LB, United Kingdom*

[2] *Department of Computer Science, University of Oxford, Oxford OX1 3QD, United Kingdom*

[3] *Institute of Biomedical Engineering, Department of Engineering Science, University of Oxford, Oxford OX3 7DQ, United Kingdom*

[4] *School of Mathematical Sciences, Queensland University of Technology, Brisbane QLD 4001, Australia*

Structural heterogeneity constitutes one of the main substrates influencing impulse propagation in living tissues. In cardiac muscle, improved understanding on its role is key to advancing our interpretation of cell-to-cell coupling, and how tissue structure modulates electrical propagation and arrhythmogenesis in the intact and diseased heart. We propose fractional diffusion models as a novel mathematical description of structurally heterogeneous excitable media, as a mean of representing the modulation of the total electric field by the secondary electrical sources associated with tissue inhomogeneities. Our results, validated against in-vivo human recordings and experimental data of different animal species, indicate that structural heterogeneity underlies many relevant characteristics of cardiac propagation, including the shortening of action potential duration along the activation pathway, and the progressive modulation by premature beats of spatial patterns of dispersion of repolarization. The proposed approach may also have important implications in other research fields involving excitable complex media.

Keywords: fractional diffusion — Riesz potential — cardiac tissue — structural heterogeneity — electrical propagation — electrotonic effects — dispersion of repolarization

[a] Corresponding author

I. INTRODUCTION

In biological tissues, the extent to which electrical propagation is influenced by the complex topology of the underlying media remains unclear. The spatial complexity of a medium can impose geometric constraints on transport processes on all length scales, which can fundamentally alter the laws of standard diffusion [1, 2]. However, conventional modeling techniques represent these tissues as continuum media with spaced averaged properties, assuming a negligible contribution of their composite microstructure in modulating electrical conduction. In the particular case of cardiac muscle, and while many mechanistic findings have been obtained using these traditional approaches, their limitations to characterize tissue structure are well acknowledged, especially under pathological conditions [3]. New modeling techniques are thus needed to promote our current understanding on the influence of tissue heterogeneity on cardiac wavefront propagation, and therefore on its role in the initiation and maintenance of cardiac arrhythmias, as to investigate novel methods and therapies for their termination.

The fundamental modeling unit in understanding the propagation of electrical excitation is the cable equation. It describes the electrical propagation of an axial current along a thin fiber consisting of a homogeneous collection of excitable cells connected via gap junctions [4]. The model is constructed via an electrical circuit representation of a small path of the cellular membrane and the principle of homogenization to derive a continuous equation of the form

$$\chi\left(C_m\partial_t V_m + I_{\text{ion}}\right) - \nabla\cdot\left(\sigma\nabla V_m\right) - I_{\text{stim}} = 0,$$

where V_m is the cellular transmembrane potential, and I_{ion} and I_{stim} the total transmembrane and stimulus currents, respectively. Model parameters are the tissue conductivity tensor, σ, the cell surface-to-volume ratio, χ, and the membrane capacitance, C_m.

Through electric potential theory, it is known that an excitable membrane will induce electric fields through all components of the surrounding tissue. This then forms the basis of the bidomain model of cardiac electrophysiology, that has been used extensively since its initial development by Tung [5],

$$\begin{aligned}\nabla\cdot\left(\sigma_i\nabla\phi_i\right) &= \chi\left(C_m\partial_t V_m + I_{\text{ion}}\right) - I_{\text{stim},i}, \quad \text{in } \Omega_i,\\ \nabla\cdot\left(\sigma_e\nabla\phi_e\right) &= -\chi\left(C_m\partial_t V_m + I_{\text{ion}}\right) - I_{\text{stim},e}, \quad \text{in } \Omega_e.\end{aligned}$$

The bidomain model assumes that the tissue consists of two overlapping spaces: the intracellular, Ω_i, and the extracellular, Ω_e, domains, respectively characterized by their corresponding conductivity tensors, σ_i and σ_e. Electrical propagation is described by the scalar potentials in Ω_i and Ω_e, ϕ_i and ϕ_e, where $V_m = \phi_i - \phi_e$.

The reasoning behind this model is that cardiac myocytes form collections of thin fibers that are arranged into sheet-like structures [3, 6]. Gap junctions between the myocytes preserve the cytosolic continuity, and so at a larger scale this structure can be viewed from some aspects as a homogeneous domain. On the other hand, gap junctions are known to have a much larger resistance compared to cytoplasm, and may be a source of discontinuous propagation on a local scale [7]. Remodeling in gap junctions distribution and connexin expression may also occur under disease conditions [8, 9], thus affecting propagation. In addition, the brick wall structure of the myocyte sheets has a marked effect on propagation. The delay in conduction depends on the number of adjacent cells connected to any given myocyte. For example, in healed infarcted canine tissue it is suggested that there exists a difference between the average number of cells connected to surrounding cells of six rather than nine or more in healthy tissue [8]. Thus the argument for treating the intracellular domain as homogeneous is questionable at least, and in the case of the extracellular space, even more doubts can be raised.

The extracellular domain is a complex mix of different tissue types, including fibrous tissue, blood vessels, collagen, fat, and interstitial pores [6]. As a particular case in point, it is known that functional fibroblasts-myocytes coupling allows fibroblasts to transduce activity between otherwise unconnected myocytes [10]. Ephaptic coupling in the narrow extracellular regions between cells may also cause large changes in ionic concentrations, that vary the electrical potential and can induce an electrical signal [11]. Furthermore, this extracellular space may change under pathological conditions, and factors as the relative volumes of intracellular and extracellular space also affect the resistance and distribution of cell-to-cell coupling [12].

Even from a mathematical point of view, the applicability of a homogenization process to cardiac tissue can be questioned. In its simplest form, homogenization assumes the domain is defined at a macroscopic scale, L, whereas the characteristic length of the heterogeneities defines a microscopic scale, $\varepsilon \ll L$. Given a conductivity tensor $\sigma(x/\varepsilon)$, homogenization studies the solution of the underlying equations as $\varepsilon \to 0$ (i.e., as heterogeneities become vanishingly small), aiming to replace the rapidly oscillating coefficients $\sigma(x/\varepsilon)$ by an effective domain characterized by constant coefficients, $\widetilde{\sigma}$. It is possible to apply these ideas to multiple scales and layered domains, but homogenization becomes increasingly difficult [13] and assumptions have to be made about the regularity of σ. However, when the number of scales becomes large, without clear separation, homogenization fails.

In this setting, fractional (non-integer) models are an appropriate alternative modeling framework [14]. Fractional spatial differential operators have been shown to incorporate the multiscale effects of transport processes taking place in heterogeneous media. Applications include the filtration of solutes in porous soils [15], diffusion of water molecules in brain tissue [16], or electrical charge transport in polymer networks [17]. It is in this context of extended structures with spatially intricate patterns that fractional models can offer insights that traditional approaches do not offer. In particular, the structural characteristics of cardiac tissue suggest fractional diffusion as an appropriate modeling framework.

In this paper, we propose a family of fractional diffusion models to describe electrical propagation in heterogeneous excitable media, analyzing their application to cardiac muscle as a representative case of composite biological tissue. These models, which represent the modulation of the electric field of an homogeneous conductor by the secondary electrical sources associated with its inhomogeneities (see Methods), are encapsulated by the general formulation

$$\partial_t V_m = -D_\alpha(-\Delta)^{\alpha/2} V_m - \frac{1}{C_m}(I_{\text{ion}} - I_{\text{stim}}), \quad 1 < \alpha \leq 2, \tag{1}$$

$$\partial_t \mathbf{y} = \mathbf{f}(V_m, \mathbf{y}), \quad I_{\text{ion}} = \mathbf{g}(V_m, \mathbf{y}), \tag{2}$$

where $(-\Delta)^{\alpha/2}$ is the fractional Laplacian operator. For the ease of presentation of these novel ideas, we concentrate on the case of isotropic conduction, so that for $\alpha = 2$ it recovers the standard monodomain formulation. This can be modified appropriately in terms of Riesz fractional derivatives, which allow for consideration of anisotropy [18]. The propagation model given by equation (1) for the transmembrane potential V_m is coupled to the system of ordinary differential equations (2), describing the cellular electrophysiological dynamics. We will focus our analysis on the upper part of the $1 < \alpha \leq 2$ range, since we hypothesize this represents a tissue with a moderate-to-medium level of structural heterogeneity.

Our fractional models of electrical propagation in cardiac tissue are validated against in-vivo human recordings and experimental data of different animal species, offering novel insights on clinically relevant mechanisms of wavefront conduction, namely action potential (AP) shortening along the pathway of activation and the modulated dispersion of repolarization. Whereas the former is considered a protective mechanism of the intact heart [19, 20], the latter relates how recovery patterns are affected by a premature stimulation of the tissue [19, 21, 22]. Hence, our results indicate the use of fractional diffusion models as a powerful tool to promote our current interpretation of the role of tissue inhomogeneities in modulating cardiac electrophysiology. The proposed approach may have, as well, important implications in unraveling the many facets of structural heterogeneity in other research fields where electrical propagation is highly influenced by complex media, such as soft muscle or neural tissue.

II. RESULTS

A. Role of Tissue Inhomogeneities in Myocardial Depolarization

The depolarization of a cardiomyocyte is characterized by an initial deviation from its resting membrane potential, known as the AP foot, then followed by the rapid AP upstroke. Probably the most comprehensive experimental study to date on the effects of tissue structure in this AP phase is still the work of Spach *et al.* [23], where the authors investigated the impact of wavefront propagation in the depolarization of canine cardiac tissue.

Figure 1A illustrates the depolarization wavefront presented in the aforementioned study during longitudinal propagation (black dashed line), compared to simulated waveforms using a biophysically detailed canine AP model [24]. Standard diffusion ($\alpha = 2$, red) yields the narrowest AP foot, with increasing foot width for decreasing fractional powers ($\alpha = 1.75$, green; $\alpha = 1.5$, blue). In particular, the value of $\alpha = 1.75$ nicely replicates the observed experimental AP foot of this ventricular preparation, whereas standard diffusion underestimates its width and morphology. Furthermore, fractional diffusion only induced a small decrease in AP amplitude when compared to standard diffusion (≈ 2.4 mV for both $\alpha = 1.75$ and $\alpha = 1.5$).

Spach *et al.* further characterized the role of wavefront conduction in depolarization by analyzing the $V_m - dV_m/dt$ phase-plane trajectories (Fig. 1B, inset). During longitudinal propagation, the majority of their ventricular and atrial impalements exhibited concave trajectories in the phase portrait ($n = 40$, 80%), indicating a deviation of the AP foot from exponential growth (that is, a linear $V_m - dV_m/dt$ relationship). The rest of the preparations displayed mixed concave/convex trajectories, but all deviated from linearity. Figure 1B shows the phase-plane trajectories in the canine model obtained for different α. Whilst standard diffusion produces a completely linear phase portrait ($\alpha = 2$, red), fractional diffusion yields profiles with increasing degree of concavity for decreasing α ($\alpha = 1.75$, green; $\alpha = 1.5$, blue). The mean experimental deviation of maximum dV_m/dt from linearity was -15.1 V/s in ventricular muscle.

This separation was quantified for the fractional diffusion models, resulting in -14.5 V/s for $\alpha = 1.75$ and -34.9 V/s for $\alpha = 1.5$. These results indicate that the depolarization dynamics of this particular experiment can be very well approximated by a fractional power close to $\alpha = 1.75$. Moreover, although the actual range of deviation from linearity was not provided in their study, the authors classified their ventricular impalements as exhibiting "minor", "moderate", and "considerable" concavity degrees (respectively, 9%, 27% and 64% of ventricular preparations, $n = 22$). This classification suggests that fractional powers $\alpha < 1.75$ (resulting in more pronounced concavities) can also be viable in healthy myocardium. In this regard, neonatal monolayers and newborn tissues, richer in microvasculature and discontinuities, exhibited even larger degrees of concavity than adult myocardium [23].

Peak value distributions for the three principal currents during depolarization are depicted in Fig. 2 for human [25] and canine [24] cell models. Despite model specific magnitudes, almost constant profiles are found for all currents in the case of standard diffusion ($\alpha = 2$, red), only influenced by the stimulus and distal boundary sites. However, the effects of fractional diffusion ($\alpha = 1.75$, green; $\alpha = 1.5$, blue) on the AP foot yield a wider range of influence for these regions. Peak magnitudes of the fast sodium, I_{Na}, and the transient outward current, I_{to}, were reduced in both models, thus leaving upstroke amplitude almost unaffected through the tissue. These results were also consistent with those in the description of rabbit electrophysiology [26]. Conversely, the behavior of the L-type calcium current, I_{CaL}, was model dependent, exhibiting a modest decrease in dog, whilst a small increase in human and rabbit models. No significant changes were observed in the rest of transmembrane currents.

B. The Inverse AT-APD Relationship

Due to its tight association with the onset of proarrhythmic substrates, the understanding of spatial patterns of AP duration (APD) is a major concern in cardiac electrophysiology. A compelling mechanism of the intact heart, reported in multiple studies and different species, is the shortening of APD during propagation, also known as the inverse AT-APD relationship. To better illustrate this aspect, the left column of Fig. 3 provides representative experimental data for in-vivo human [19], dog [20], and isolated rabbit hearts [27].

The contribution of tissue inhomogeneities, as modeled by fractional diffusion, to APD dispersion (ΔAPD) was investigated in tissue cables for biophysically detailed models of human [25], dog [24] and rabbit [26], as shown in the right column of Fig. 3. Standard diffusion ($\alpha = 2$, red) yields moderate ΔAPD values, regardless of cell type. More remarkable is the fact that, for all cell models, ΔAPD distributions turn into nearly constant profiles once the domain size becomes comparable to the AP wavelength [28]. On the other hand, ΔAPD increasingly grows for decreasing fractional power ($\alpha = 1.75$, green; $\alpha = 1.5$, blue), more closely resembling the ΔAPD profiles reported experimentally.

Two mechanisms are responsible for the larger extent of APD shortening associated with the fractional diffusion models. First, cell-to-cell electrotonic load is substantially larger at all sites for fractional compared to standard diffusion, as illustrated in Fig. 4 for the human and canine cellular models. Within the stimulated region (Fig. 4 A,B), the current is large and positive, which lengthens APD. At the boundary (Fig. 4 E,F), the current is large and negative, contributing to APD shortening [28]. Electrotonic currents are also larger for cell models with a sharper repolarization phase (see individual APs in Fig. 3), in agreement with previous results [28]. Despite specific AP morphology, the influence of fractional diffusion in increasing repolarization effects was consistent for all the studied cell models. Additionally, the above described effects of fractional diffusion on tissue depolarization also leave a smaller bulk of depolarizing current opposed to the increased electrotonic load over a wider extent of the domain, hence also contributing to APD shortening at distal locations of the tissue.

The interplay between these two mechanisms is better illustrated in Fig. 5, where experimental APD patterns in neonatal rat monolayers [29] are analyzed against standard and fractional models of wavefront propagation. The neonatal rat parameterization [30] for the phenomenological model in [31] was used as cellular model, and a value of $\alpha = 1.5$ was chosen for the fractional diffusion model due to the substantial degree of tissue inhomogeneities in cell cultures, as previously mentioned [23]. Although standard diffusion correctly reproduces the activation sequence, the resulting APD distribution is almost constant through the tissue (Fig. 5, second column). Instead, the increased electrotonic load plus the modulation of depolarizing currents in fractional diffusion result in a larger extent of APD shortening, as depicted in the third column of Fig. 5.

To further appreciate the contribution of the depolarization phase to APD shortening, we also explored a modified model parameterization yielding a supplementary reduction in the model total inward current during its AP foot (see Methods). Results for fractional diffusion are contained in the last column of Fig. 5, showing a closer agreement in replicating the APD profile, whereas standard diffusion still yields an almost constant APD distribution (data not shown). Therefore, and even though these results do not exclude additional factors in the observed experimental APD patterns, they highlight the possible role that myocardial structure may have in modulating membrane currents and APD dispersion at tissue level.

C. The Modulated Dispersion of Repolarization

Another important characteristic of cardiac tissue, due to its implications in arrhythmogenesis, is the nonlinear response referred to as APD restitution. Among existing protocols, the most clinically relevant is the standard or S_1-S_2 restitution. For steady-state conditions at a fixed S_1 pacing cycle length, this protocol relates APD at any tissue point as a function of their preceding diastolic interval, $\text{APD}^n = f(\text{DI}^{n-1})$, under a premature S_2 stimulus. Here DI^{n-1}=CI-APD^{n-1} and CI is the coupling interval (time difference between S_1 and S_2 stimulations), whereas superscripts refer to the beat number.

Due to the shortening of APD during propagation, a range of restitution profiles may also exist along the path of activation. Such an effect in APD restitution has been reported in human [19] and animal [21, 22] studies. Experimental evidence for one patient with healthy ventricles is presented in Fig. 6A. For each coupling interval, local APDs from numerous ventricular sites are plotted against their preceding DIs, and a local regression line is drawn. For test beats close to the basic cycle length (right side of the panel), the regression line has a slope of -1. As the coupling interval is shortened, DIs decreased and the restitution curve acted to reduce APD dispersion. This results in the progressive flattening of regression lines known as modulated dispersion of repolarization, with electrode sites having shorter DIs exhibiting a larger APD reduction compared to electrodes sites with longer DIs [19].

The ability of the different propagation models in reproducing the modulated dispersion of repolarization was inspected for human electrophysiology [25]. Figure 6B shows results for standard diffusion ($\alpha = 2$). The APD difference between early and late activating sites is small in this case, due to the minimum role of standard diffusion in the inverse AT-APD relationship. More intriguing is the rapid inversion of DI-APD regression lines at medium and short coupling intervals, not observed in the in vivo data. Results for fractional diffusion models are also presented, for $\alpha = 1.75$ (Fig. 6C) and $\alpha = 1.5$ (Fig. 6D). As the fractional order α is decreased, not only does the APD difference between early and late activating sites increase, but the progressive flattening of regression lines is also recovered. Two factors are involved in the recovery of this gradual flattening. First, the APD decreases along the activation pathway; and secondly, there is an increased dispersion of local DIs in the tissue, as can be observed by comparison of Figs. 6B-D. Both factors are interrelated, since DI^{n-1}=CI-APD^{n-1}. Thus, the larger the APD dispersion in the basic beat, the bigger the resulting dispersion of DIs preceding the premature stimulus.

An additional property known to interact with APD restitution in the modulation of APD patterns is conduction velocity (CV) restitution [32, 33]. Equivalently to APD restitution, this relates CV as a function of their preceding DIs, $\text{CV}^n = f(\text{DI}^{n-1})$. Fractional diffusion effects on CV restitution are investigated in Fig. 7. Only slight modifications in CV restitution profiles are observed at short DIs for decreasing α, due to the increased dispersion of local DIs for the fractional diffusion models. Therefore, fractional diffusion allows the reproduction of key properties in the dispersion of repolarization in cardiac tissue, without altering other important properties of cardiac conduction.

III. DISCUSSION

Clinical, experimental, and theoretical studies have suggested that structural heterogeneity may actively modulate the course of impulse propagation and recovery of excitability in cardiac tissue [12, 23, 30, 34]. However, limitations of conventional modeling techniques hamper our ability to provide novel insights into the influence of tissue microstructure in these regards. The new modeling framework presented in this contribution aims to probe mathematical descriptions of cardiac tissue with the macroscopic effects of such structural heterogeneity. Our findings, analyzed in cellular models of human, dog, rabbit and neonatal rat electrophysiology, indicate that the secondary electrical sources created by myocardial inhomogeneities, as modeled by fractional diffusion, play a significant role in explaining a number of relevant characteristics of cardiac repolarization.

Shortening of APD along the activation path has been reported in human and different animal species [19–21, 27]. Importantly, this inverse AT-APD relationship is considered a natural protective mechanism of the intact heart [19], since as APD shortens, so does dispersion of repolarization, which is widely accepted as being arrhythmogenic [20, 35]. However, this property of wavefront propagation is not accurately reproduced by standard diffusion models of cardiac tissue, which yield almost entirely constant AT-APD distributions (Fig. 3). Our results suggest that tissue inhomogeneities assert a crucial role in the mode of action of electrotonic current flow, thus explaining the inverse AT-APD coupling and highlighting its implications as the underlying mechanism regulating the modulated dispersion of repolarization. They also indicate a tissue modulation of ionic currents acting during AP depolarization. Moreover, experimental evidences indicating a structural role of the tissue on membrane currents, and on the morphology of the initial part of the depolarizing phase, have been also reported [12, 23].

On the other hand, several guinea pig studies have suggested that regional differences in the expression of ionic currents may underlie APD shortening during propagation [21, 22]. Whereas we cannot exclude their possible contribution to total APD dispersion, other experimental studies have shown electrotonic modulation of APD dominates

the effects of intrinsic differences in cellular repolarization characteristics [36]. Although the main goal of this work was to characterize the role of tissue heterogeneities in cardiac repolarization, it will be interesting to analyze how fractional diffusion modulates existing ionic gradients in cardiac tissue, and their contribution, for instance, to the body-surface electrocardiogram.

The proposed models also represent a flexible approach to characterize the role of cardiac microstructure in electrical propagation in terms of computational tractability, since spatial discretization is retained at a mesoscopic and not subcellular scale. However, their numerical resolution can impose a number of constraints when compared to standard diffusion, since the fractional Laplacian yields full, instead of sparse, matrices. Nevertheless, new efficient techniques, that avoid the explicit calculation of the fractional operator, have been recently proposed for these types of systems [18, 37]. In particular, and for sufficiently regular geometries, the methods presented in [18] achieve the same computational cost as associated to standard diffusion.

Therefore, fractional diffusion models may have potential implications in advancing our understanding on the mechanisms of dispersion of repolarization and its modulation by premature beats, and thus vulnerability to and initiation of lethal arrhythmias. Finally, our findings indicate that fractional powers $\alpha < 2$ reproduce many interesting tissue properties in a variety of human and animal cellular models. Although we have concentrated our analysis in the upper part of its allowable range, lower values of α are nevertheless admissible. This may represent, for example, disease conditions such as fibrotic tissue, but this remains to be analyzed in much greater detail, and a rigorous methodology needs to be developed to properly estimate these values. Different imaging modalities have been recently proposed to characterize fractional diffusion transport in neural tissue [16, 38], and they might be extended as well for their application to cardiac tissue. Importantly, we are not suggesting that there should be a unique value to represent heterogeneities. Rather, we suggest that there are ranges of suitable values of α in different settings (such as healthy or diseased states), and this is consistent with important new modeling approaches centered around the concept of populations of models to represent biological variability [39, 40]. All these points will be addressed in future work.

IV. METHODS

A. Biophysical Justification of Fractional Diffusion Models in Excitable Media

Both the monodomain and the bidomain formulations of the cable equation are well accepted methodologies to describe the spread of electrical activity in excitable media [3]. The only difference between these modeling approaches and our proposed fractional diffusion models for heterogenous excitable media is the replacement of the diffusive term (which describes tissue coupling) in equation (1) by the fractional Laplacian, $(-\Delta)^{\alpha/2}$. None of the remaining terms are subject to additional changes or affected by any spatial dependence. In this section, we aim to provide a biophysical interpretation for this new coupling term, which captures the degree of structural heterogeneity in the tissue.

In a statistical sense, the fractional reaction-diffusion process given by equation (1) can be viewed as describing the probability density function of an ensemble of particles undergoing a Lévy (jump) process [1, 2]. However, a further biophysical motivation is needed for our fractional diffusion models in our context of excitable media. In order to make our justification beyond Lévy walks, we resort to potential theory. Consider a homogeneous domain in three-dimensional space with conductivity σ and a source I at point (x, y, z). Then, the electric potential ϕ satisfies the solution of

$$-\Delta\phi = \frac{I}{\sigma},$$

which at a field point (x', y', z') is given by

$$\phi(x', y', z') = \frac{1}{4\pi\sigma}\int_\Omega \frac{I}{r}\, dV,$$

where $r = \left[(x-x')^2 + (y-y')^2 + (z-z')^2\right]^{1/2}$. Thus the electric potential of a monopole $I = I_0\delta(r)$ is given by

$$\phi_m(r) = \frac{I_0}{4\pi\sigma r}. \tag{3}$$

Equivalently, the electric potential associated with a dipole (two adjacent monopoles of equal and opposite sign, separated by a small distance d) is, for $r \gg d$

$$\phi_d(r) = \frac{I_0}{4\pi\sigma}\frac{d\cos\theta}{r^2}, \tag{4}$$

where θ is the polar angle between the dipole and the field point.

It is known that biological tissue gives rise to volume conductors that are inhomogeneous in essence, so that inhomogeneities can drive secondary sources once a primary source has established a field and current flows across the interface separating regions of different conductivities [4]. The contribution from those secondary sources can be written as

$$\phi_p(r) = \frac{1}{4\pi\sigma_p} \sum_i \oint_{S_i} \delta\sigma_i \cdot \phi_i \frac{\vec{a}_r \cdot d\vec{S}}{r^2},$$

where S_i denotes the i-th surface on which a discontinuity in conductivity, $\delta\sigma_i$, occurs. Here, $\vec{a}_r$ is the unit radius vector from source to field and $\oint_{S_i}$ represents the integral over surface S_i.

These secondary sources arising due to tissue inhomogeneities can be seen as a dipole modulation of a monopole, in that by letting the $\delta\sigma_i$ go to zero we recover the original monopole, but at the other extreme we retrieve a dipole. This suggests a dependence on r ranging from $1/r$ to $1/r^2$. This insight allows to make the connection to fractional models in terms of Riesz potential theory [41, 42]. In $\mathbb{R}^N$, the fractional Laplacian can be written as

$$(-\Delta)^{\alpha/2}\phi = C_\alpha \int_{\mathbb{R}^N} \frac{\phi(r) - \phi(r')}{\|r - r'\|^{N+\alpha}}\, dr'$$

on a bounded domain with zero Dirichlet boundary conditions, while the case of reflecting boundary conditions has recently been considered [43]. Now, the solution of

$$(-\Delta)^{\alpha/2}\phi = f,$$

under the assumption that f is sufficiently regular and has compact support (so that it vanishes at infinity), can be written as

$$\phi(r) = (-\Delta)^{-\alpha/2} f = \frac{1}{C_\alpha} \int_{\mathbb{R}^N} \frac{f(r')}{\|r - r'\|^{N-\alpha}}\, dr',$$

where

$$C_\alpha = \frac{\pi^{N/2}\, 2^\alpha\, \Gamma(\frac{\alpha}{2})}{\Gamma\left(\frac{N-\alpha}{2}\right)}$$

and $\Gamma(\cdot)$ denotes the Gamma function. So, for $N = 3$ and $f = I_0\delta(r)/\sigma$, then for $\alpha = 2$, $C_\alpha = 4\pi$ and $\phi(r) \sim 1/r$, which is consistent with the monopole described in equation (3). Equivalently, for $\alpha = 1$ the dipole dependence $\phi(r) \sim 1/r^2$ in equation (4) is recovered. Intermediate values $1 < \alpha \leq 2$ can thus be interpreted as a smooth transition between these two types of electric potentials, representing a biological tissue with increasing degree of inhomogeneities as α approaches its ballistic lower limit. Analogous continuity arguments have been used in other applications of fractional calculus to electrostatic theory [44–46]. Similarly, fractional models have been effectively applied to describe the presence of impurities in semiconductor heterostructures [47], where the generalization of fractal conductance, depending on restrain conditions in charge movement, has been also proposed [48, 49].

B. Parameterization of Models

Macroscopic properties of cardiac tissue, such as CV, must be captured by the specific propagation model regardless of its mathematical description. The diffusion coefficient D_α in equation (1) was thus adjusted for the fractional models to match the CV in standard diffusion ($\alpha = 2$), as measured in the center of tissue cables of 2 cm length. For standard diffusion, a diffusion coefficient of 0.1 cm^2/s was used for neonatal rat models [30], whereas values of 1.2, 1.0 and 1.4 cm^2/s were used for human, dog and rabbit models, respectively, to yield a CV of 70, 58 and 67 cm/s as experimentally reported.

All cellular models representing the species dependent I_{ion} term in equation (2) were coded using their curated implementations in the CellML repository (`http://models.cellml.org/electrophysiology`). Model parameters were only modified in the neonatal rat model [30, 31], by using $\tau_{so1} = 45$ (+27%) and $\tau_{o2} = 15$ (+50%), in order to match experimental APD values close to the stimulus site [29]. The main effect of a wider AP foot in the dynamics of this simplified model is to increase the decay of its w gate during depolarization, which controls the model slow inward current. To further accentuate this mechanism, we considered an additional model parameterization with faster w inactivation. This was achieved by setting $w^*_\infty = 0.5$ (-41%), $u^-_w = 0.1$ (+90%), $\tau^-_{w1} = 35$ (-34%), $k^-_w = 2.5$ (-96%). Numbers in parentheses indicate percent of variation with respect the original model parameterization.

C. Protocols for Validation against Experimental Data

Tissue models were initialized with single-cell steady-state conditions at the specified cycle lengths, and paced as indicated in the main text until the relative difference in ΔAPD was less than 0.5% in two consecutive heart beats. AT was determined at the steepest upstroke of the AP, whereas RT was quantified at a specified per cent of repolarization (80% for neonatal cell cultures, 90% for the biophysically detailed cell models, matching reported experimental conditions). APD was measured as the difference between the repolarization and activation times. Dispersion in any of these values was measured as the difference between the maximum and minimum values obtained over the entire domain.

APD restitution curves were calculated in one-dimensional cables of 4 cm length. The cable was paced until steady-state at one end with a stimulus of strength 2×diastolic threshold and a cycle length of 1000 ms, then introducing test pulses over a range of different coupling intervals. The resulting DI-APD pairs were computed for all points in the tissue.

D. Numerical Techniques

One-dimensional simulations were performed using a semi-implicit Fourier spectral method [18], whereas a finite differences discretization of the Laplacian in polar coordinates, raised to the fractional power $\alpha/2$, was used for the numerical solution of tissue monolayers. Temporal and spatial resolutions of $\Delta\ t = 0.0025$ ms and $\Delta\ x = 1/64$ cm $\approx 150\ \mu$m were used in all models. Non-flux boundary conditions were imposed to ensure conservation of charge.

[1] Metzler R. & Klafter J. The random walk's guide to anomalous diffusion: A fractional dynamics approach. *Phys Rep* **339**, 1–77 (2000)

[2] Metzler R. & Klafter J. The restaurant at the end of the random walk: recent developments in the description of anomalous transport by fractional dynamics. *J Phys A: Math Gen* **37**, R161–R208 (2004)

[3] Clayton R.H. *et al.* Models of cardiac tissue electrophysiology: Progress, challenges and open questions. *Prog Biophys Mol Biol* **104**, 22–48 (2011)

[4] Plonsey R. & Barr R. *Bioelectricity: A quantitative approach*, third edition, Springer, New York (2007)

[5] Tung L. A bi-domain model for describing ischemic myocardial d-c potentials. *PhD Dissertation*, Massachussets Institute of Technology, Massachussets (1978)

[6] Frank J. & Langer, G. The myocardial interstitium: its structure and its role in ionic exchange. *J Cell Biol* **60**, 586–601 (1974)

[7] Diaz P.J., Rudy Y. & Plonsey R. Intercalated discs as a cause for discontinuous propagation in cardiac muscle: a theoretical simulation. *Ann Biomed Eng* **11**, 177–189 (1983)

[8] Luke R.A. & Saffitz J.E. Remodeling of ventricular conduction pathways in healed canine infarct border zones. *J Clin Invest* **87**, 1594–1602 (1991)

[9] Severs N.J., Bruce A.F., Dupont E. & Rothery S. Remodelling of gap junctions and connexin expression in diseased myocardium. *Cardiovasc Res* **80**, 9–19 (2008)

[10] Camelliti P., Green C., LeGrice I. & Kohl P. Fibroblast network in rabbit sinoatrial node: structural and functional identification of homogeneous and heterogeneous cell coupling. *Circ Res* **94**, 828–835 (2004)

[11] Sperelakis N. & McConnell K. Electric field interactions between closely abutting excitable cells. *IEEE Eng Med Biol Mag* **21**, 77–89 (2002)

[12] Spach M.S. *et al.* The discontinuous nature of propagation in normal canine cardiac muscle. Evidence for recurrent discontinuities of intracellular resistance that affect the membrane currents. *Circ Res* **48**, 39–54 (1981)

[13] Pavliotis G.A. & Stuart A.M. *Multiscale methods. Averaging and homogenization*, Springer, New York (2008)

[14] Alliare G. & Briane M. Multiscale convergence and reiterated homogenisation. *Proc R Soc Edinb Sect A-Math*, **126**, 297–342 (1996)

[15] Benson D.A., Wheatcraft S.W. & Meerschaert M.M. Application of a fractional advection-dispersion equation. *Water Resour Res* **36**, 1403–1412 (2000)

[16] Capuani S.*et al.* Spatio-temporal anomalous diffusion imaging: results in controlled phantoms and in excised human meningiomas. *Magn Reson Imaging*, **31**, 359–365 (2013)

[17] Hernández-Labrado G.R., Contreras-Donayre R.E., Collazos-Castro J.E. & Polo J.L. Subdiffusion behavior in poly(3,4-ethylenedioxythiophene): Polystyrene sulfonate (PEDOT:PSS) evidenced by electrochemical impedance spectroscopy. *J Electroanal Chem* **659**, 201–204 (2011)

[18] Bueno-Orovio A., Kay D. & Burrage K. Fourier spectral methods for fractional-in-space reaction-diffusion equations. *J Comput Phys*, submitted (2012)

[19] Hanson B. *et al.* Interaction of activation-repolarization coupling and restitution properties in humans. *Circ Arrhythmia Electrophysiol* **2**, 162–170 (2009)

[20] Opthof T., Coronel R. & Janse M.J. Is there a significant transmural gradient in repolarization time in the intact heart? Repolarization gradients in the intact heart. *Circ Arrhythmia Electrophysiol* **2**, 89–96 (2009)

[21] Laurita K.R., Girouard S.D. & Rosenbaum D.S. Modulation of ventricular repolarization by a premature stimulus. Role of epicardial dispersion of repolarization kinetics demonstrated by optical mapping of the intact guinea pig heart. *Circ Res* **79**, 493–503 (1996)

[22] Laurita K.R., Girouard S.D., Akar F.G. & Rosenbaum D.S. Modulated dispersion explains changes in arrhythmia vulnerability during premature stimulation of the heart. *Circulation* **98**, 2774–2780 (1998)

[23] Spach M.S., Heidlage J.F., Dolber P.C. & Barr R.C. Extracellular discontinuities in cardiac muscle: evidence for capillary effects on the action potential foot. *Circ Res* **83**, 1144–1164 (1998)

[24] Decker K.F., Heijman J., Silva J.R., Hund T.J. & Rudy Y. Properties and ionic mechanisms of action potential adaptation, restitution, and accommodation in canine epicardium. *Am J Physiol Heart Circ Physiol* **296**, H1017–H1026 (2009)

[25] ten Tusscher K.H.W.J. & Panfilov A.V. Alternans and spiral breakup in a human ventricular tissue model. *Am J Physiol Heart Circ Physiol* **291**, H1088–H1100 (2006)

[26] Mahajan A. *et al.* A rabbit ventricular action potential model replicating cardiac dynamics at rapid heart rates. *Biophys J* **94**, 392–410 (2008)

[27] Costard-Jäckle A., Goetsch B., Antz M. & Franz M.R. Slow and long-lasting modulation of myocardial repolarization produced by ectopic activation in isolated rabbit hearts. Evidence for cardiac "memory". *Circulation* **80**, 1412–1420 (1989)

[28] Cherry E.M. & Fenton F.H. Effects of boundaries and geometry on the spatial distribution of action potential duration in cardiac tissue. *J Theor Biol* **285**, 164–176 (2011)

[29] Badie N. & Bursac N. Novel micropatterned cardiac cell cultures with realistic ventricular microstructure. *Biophys J* **96**, 3873–3885 (2009)

[30] Kim J.M., Bursac N. & Henriquez C.S. A computer model of engineered cardiac monolayers. *Biophys J* **98**, 1762–1771 (2010)

[31] Bueno-Orovio A., Cherry E.M. & Fenton F.H. Minimal model for human ventricular action potentials in tissue. *J Theor Biol* **253**, 544–560 (2008)

[32] Fenton F.H., Cherry E.M., Hastings H.M. & Evans S.J. Multiple mechanisms of spiral wave breakup in a model of cardiac electrical activity. *Chaos* **12**, 852–892 (2002)

[33] Cherry E.M. & Fenton F.H. Suppression of alternans and conduction blocks despite steep APD restitution: electrotonic, memory, and conduction velocity restitution effects. *Am J Physiol Heart Circ Physiol* **286**, H2332–H2341 (2004)

[34] Engelman Z.J., Trew M.L. & Smaill B.H. Structural heterogeneity alone is a sufficient substrate for dynamic instability and altered restitution. *Circ Arrhythm Electrophysiol* **3**,195–203 (2010)

[35] Coronel R., Wilms-Schopman F.J.G., Opthof T. & Janse M.J. Dispersion of repolarization and arrhythmogenesis. *Heart Rhythm* **6**, 537–543 (2009)

[36] Myles R.C., Bernus O., Burton F.L., Cobbe S.M. & Smith G.L. Effect of activation sequence on transmural patterns of repolarization and action potential duration in rabbit ventricular myocardium. *Am J Physiol Heart Circ Physiol* **299**, H1812–H1822 (2010)

[37] Burrage K., Hale N. & Kay D. An efficient implicit FEM scheme for fractional-in-space reaction-diffusion equations. *SIAM J Sci Comput* **34**, A2145–A2172 (2012)

[38] Magin R.L., Ingo C., Colon-Perez L., Triplett W. & Mareci T.H. Characterization of anomalous diffusion in porous biological tissues using fractional order derivatives and entropy. *Microporous Mesoporous Mat* http://dx.doi.org/10.1016/j.micromeso.2013.02.054 (2013)

[39] Britton O.J. *et al.* Experimentally-calibrated population of models predicts and explains inter-subject variability in cardiac cellular electrophysiology. *Proc Natl Acad Sci USA*, 10.1073/pnas.1304382110 (2013)

[40] Walmsley J. *et al.* mRNA expression levels in failing human hearts predict cellular electrophysiological remodeling: a population-based simulation study. *PLoS ONE* **8**, e56359 (2013)

[41] Riesz M. L'intégrale de Riemann-Liouville et le problème de Cauchy. *Acta Mathematica* **81**, 1–222 (1949)

[42] Karlsen K.H., Petitta F. & Ulusoy S. A duality approach to the fractional Laplacian with measure data. *Publ Mat* **55**, 151–161 (2011)

[43] Kay D., Turner I., Cusimano N. & Burrage K. Reflections from a boundary: reflecting boundary conditions for space-fractional partial differential equations on bounded domains. *SIAM J Sci Comput*, submitted (2013)

[44] Engheta N. On fractional calculus and fractional multipoles in electromagnetism. *IEEE Trans Antennas Propag* **44**, 554–566 (1996)

[45] Engheta N. Electrostatic 'fractional' image methods for perfectly conducting wedges and cones. *IEEE Trans Antennas Propag* **44**, 1565–1574 (1996)

[46] Engheta N. On the role of fractional calculus in electromagnetic theory. *IEEE Antennas Propag Mag* **39**, 35–46 (1997)

[47] Mikhailov I.D., Betancur F.J., Escorcia R.A. & Sierra-Ortega J. Shallow donors in semiconductor heterostructures: Fractal dimension approach and the variational principle. *Phys Rev B* **67**, 115317 (2003)

[48] Ketzmerick R. Fractal conductance fluctuations in generic chaotic cavities. *Phys Rev B* **54**, 10841–10844 (1996)

[49] Marlow C.A. *et al.* Unified model of fractal conductance fluctuations for diffusive and ballistic semiconductor devices. *Phys Rev B* **73**, 195318 (2006)

ACKNOWLEDGMENTS

This publication is based on work supported by Award No. KUK-C1-013-04, made by King Abdullah University of Science and Technology (KAUST). BR holds Medical Research Council Career Development, Industrial Partnership, and Centenary awards. We thank Dr. Ben Hanson (University College of London) for providing the experimental data for Figure 6.

AUTHOR CONTRIBUTIONS

ABO, DK, VG, BR and KB, conception and design of research; ABO and KB, contributed with analytical tools; ABO, performed experiments and analyzed data; ABO and KB, drafted manuscript; ABO, DK, VG, BR and KB, revised and approved final version of manuscript.

COMPETING FINANCIAL INTERESTS

The authors declare no competing financial interests.

FIGURE LEGENDS

Figure 1. Effects of fractional diffusion on tissue depolarization, recorded in the center of a 4 cm cable in length. A: Fractional propagation models (α=1.75, green; α=1.5, blue) significantly increase action potential foot width when compared to standard diffusion (α=2, red). Experimental data (dashed black line) illustrate a representative depolarization wavefront in healthy canine ventricular myocardium during longitudinal propagation. B: Phase-plane trajectories during depolarization for the different values of the fractional power α, indicating a concave deviation from linearity in the fractional models as experimentally reported (inset). Experimental data modified from [23].

Figure 2. Peak value distributions (μA/μF) for the three predominant currents during depolarization for human (left) and canine (right) cell models, measured in a tissue cable of 4 cm length stimulated at its boundary. Despite displaying the same magnitudes at the distal boundary, fractional propagation models (α=1.75, green; α=1.5, blue) significantly increase the range of influence of this region compared to standard diffusion (α=2, red).

Figure 3. Left: experimental AT-APD relationships in human (A), canine (C) and rabbit (E) cardiac tissue (modified from [19, 20, 27]). Linear regression fits indicate an inverse correlation between both magnitudes. Right: fractional effects in APD dispersion for human (B), dog (D) and rabbit (F) cell models. Color indicates fractional derivative order (α=2, red; α=1.75, green; α=1.5, blue). Solid and dashed lines denote shorter and longer tissue cables (2 and 4 cm length, halved for rabbit simulations), stimulated at their left boundary (2×threshold; 2 ms duration; 1 Hz pacing for human and canine, 2 Hz for rabbit). APD dispersion is substantially larger in the fractional diffusion models, closer in magnitude and morphology to the experimental values. Insets show single-cell action potentials for the different cell models (horizontal bars scale, 100 ms; vertical bars, 50 mV).

Figure 4. Diffusive repolarization currents for human and canine cell models at proximal (A,B), intermediate (C,D) and distal (E,F) locations from stimulus site, measured in a tissue cable of 4 cm length stimulated at its boundary. Coupling currents are substantially increased at all sites for fractional models (α=1.75, green; α=1.5, blue) compared to standard diffusion (α=2, red).

Figure 5. Activation sequence (A1) and APD distribution (B1) in isotropic neonatal rat monolayers (from [29], with permission). The experiment consists in a circular isotropic monolayer of 17 mm of diameter, stimulated at its center (1.2×threshold; 10 ms duration; 2 Hz pacing). All tissue models are able to replicate the activation map (A2-A4). However, standard diffusion produces an almost constant APD distribution (B2). Fractional diffusion models yield APD profiles in better agreement with the experimental results (B3-B4). Representative action potential traces demonstrate decrease in APD with distance from the pacing site for the fractional models.

Figure 6. Global DI-APD relationship changing with premature coupling interval in a standard restitution protocol. A: Experimental data from multiple recording sites from healthy human endocardium (modified from [19]). Linear regression lines are shown for APD versus DI at each test coupling interval, exhibiting a progressive flattening of slope as the coupling interval shortens. B: Global DI-APD dependence in a simulated cable of human cardiac tissue of 4 cm length using standard diffusion (α=2). Not only is dispersion between early and late APD restitution curves small, but regression lines manifest a rapid inversion of slopes at short coupling intervals. C, D: Global DI-APD dependence for fractional diffusion models (α=1.75 and α=1.5, respectively). The separation between early and late APD restitution curves increases for decreasing fractional order α, also recovering the progressive flattening of regression lines.

Figure 7. Conduction velocity restitution profiles in a human model of cardiac electrophysiology, measured at proximal (A), medial (B) and distal (C) locations in a tissue cable of 4 cm length. Recording sites are, respectively, located at 1, 2 and 3 cm from the stimulated boundary. Insets provide details of CV restitution at short diastolic intervals, whereas color indicates derivative order (α=2, red; α=1.75, green; α=1.5, blue).

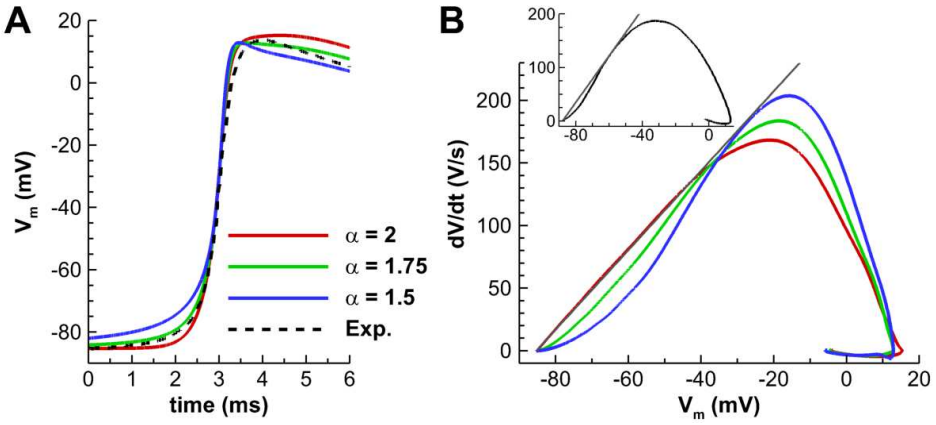
A
B
V_m (mV)
time (ms)
α = 2
α = 1.75
α = 1.5
Exp.
dV/dt (V/s)
V_m (mV)

FIG. 1.

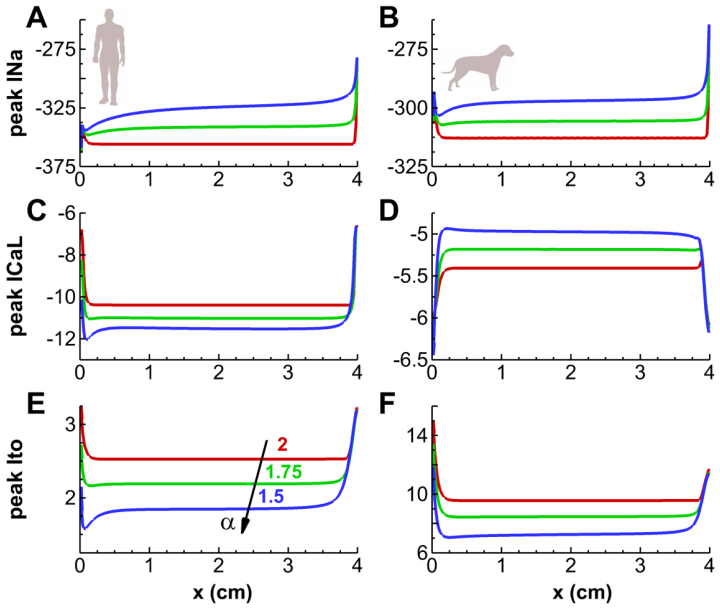
A
B
C
D
E
F
peak INa
peak ICaL
peak Ito
2
1.75
1.5
α
x (cm)
x (cm)

FIG. 2.

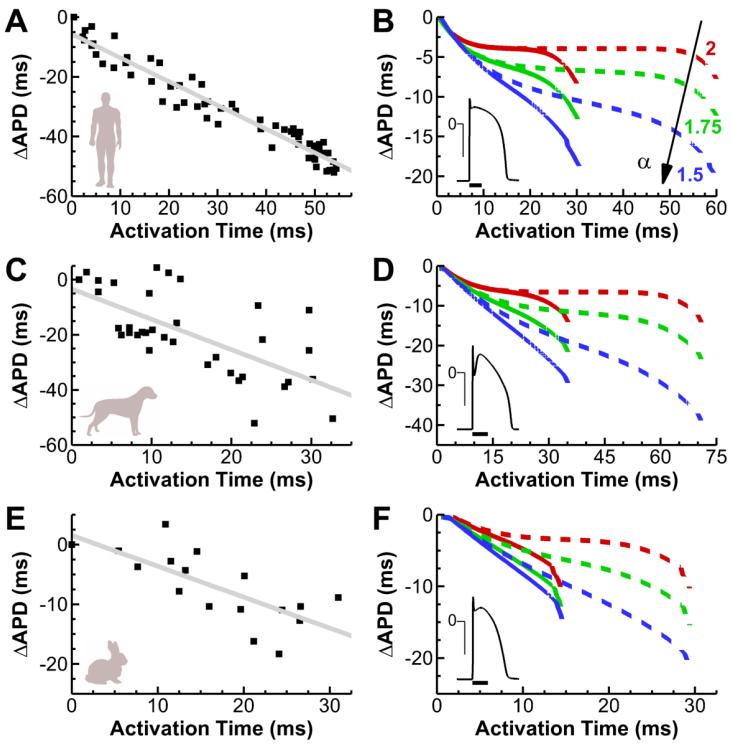
A
B
C
D
E
F
ΔAPD (ms)
Activation Time (ms)
2
1.75
1.5
α

FIG. 3.

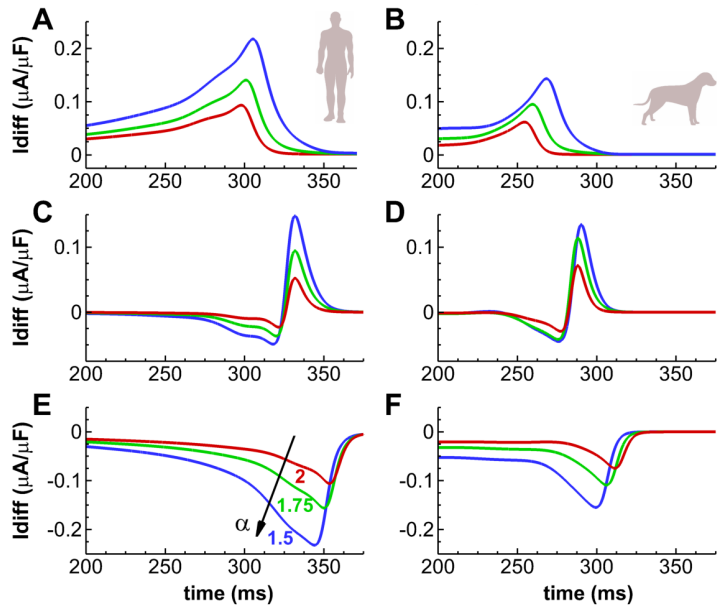
A
B
C
D
E
F
Idiff (μA/μF)
time (ms)
2
1.75
1.5
α

FIG. 4.

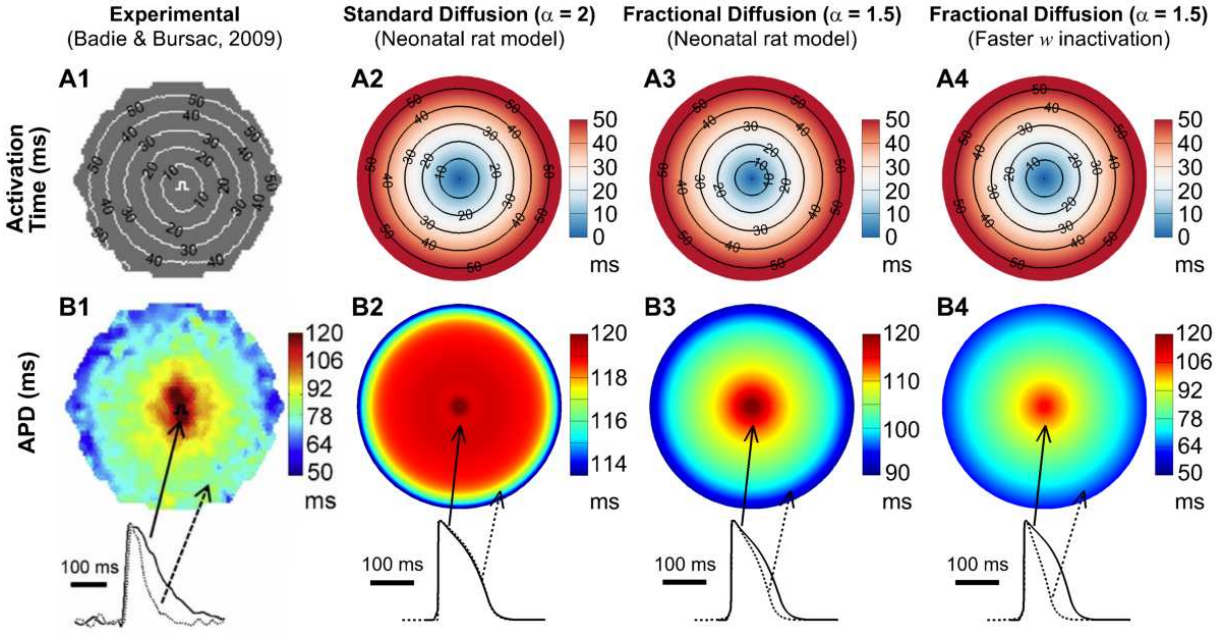
Experimental
(Badie & Bursac, 2009)
Standard Diffusion (α = 2)
(Neonatal rat model)
Fractional Diffusion (α = 1.5)
(Neonatal rat model)
Fractional Diffusion (α = 1.5)
(Faster w inactivation)
A1
A2
A3
A4
Activation Time (ms)
50 40 30 20 10 0 ms
B1
B2
B3
B4
APD (ms)
120 106 92 78 64 50 ms
120 118 116 114 ms
120 110 100 90 ms
120 106 92 78 64 50 ms
100 ms

FIG. 5.

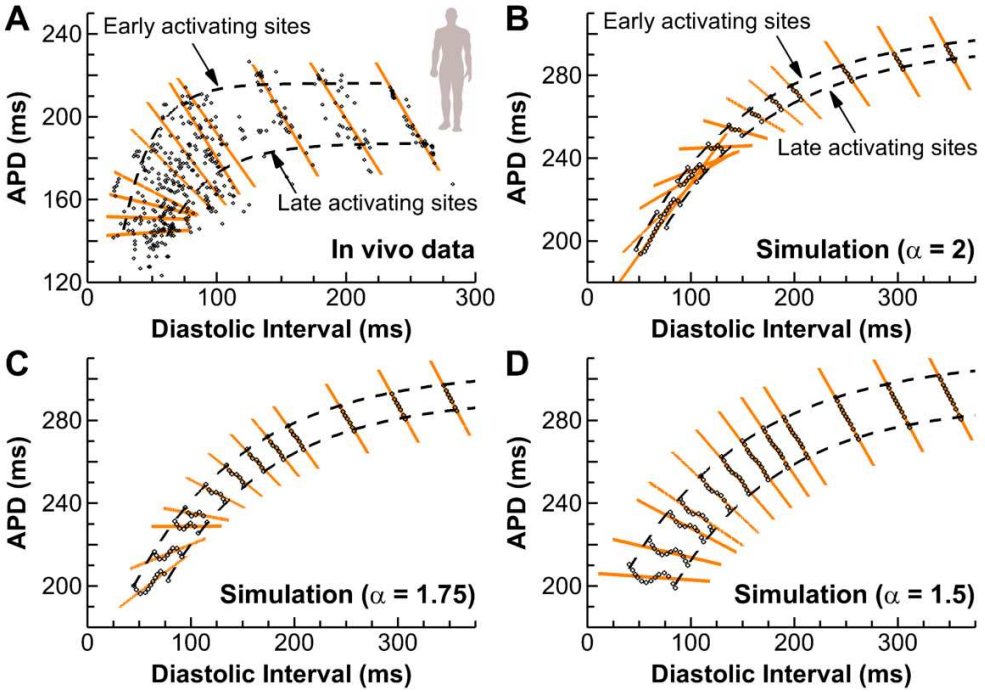
A
Early activating sites
Late activating sites
In vivo data
APD (ms)
Diastolic Interval (ms)
B
Simulation (α = 2)
C
Simulation (α = 1.75)
D
Simulation (α = 1.5)

FIG. 6.

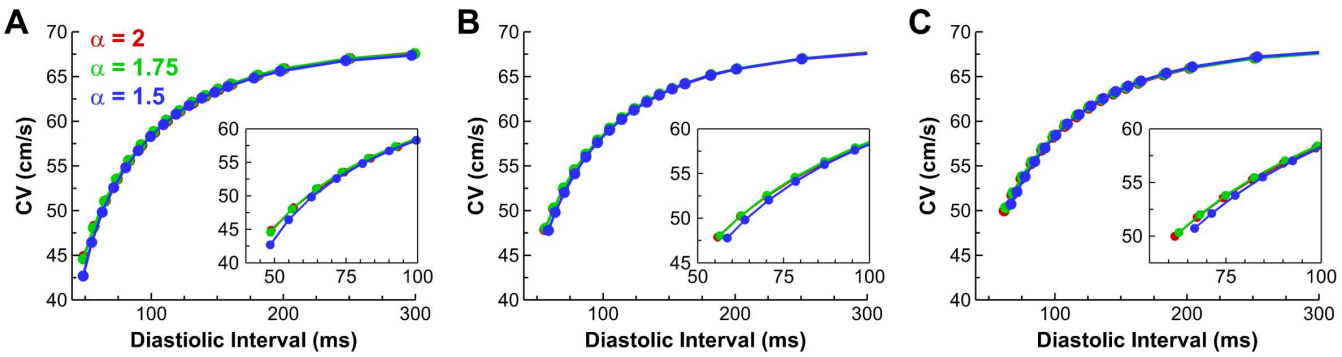
A
α = 2
α = 1.75
α = 1.5
CV (cm/s)
Diastiolic Interval (ms)
B
CV (cm/s)
Diastolic Interval (ms)
C
CV (cm/s)
Diastolic Interval (ms)

FIG. 7.

RECENT REPORTS

13/12	Switch on, switch off: stiction in nanoelectromechanical switches	Wagner Vella
13/13	Pinning, de-pinning and re-pinning of a slowly varying rivulet	Paterson Wilson Duffy
13/14	Travelling-wave similarity solutions for a steadily translating slender dry patch in a thin fluid film	Yatim Duffy Wilson
13/15	A stochastic model for early placental development	Cotter Klika Kimpton Collins Heazell
13/16	Experimentally-calibrated population of models predicts and explains inter-subject variability in cardiac cellular electrophysiology	Britton Bueno-Orovio Van Ammel Lu Towart Gallacher Rodriguez
13/17	Elastometry of deflated capsules elastic moduli from shape and wrinkle analysis	Knoche Vella Aumaitre Degen Rehage Cicuta Kierfeld
13/18	The effect of a concentration-dependent viscosity on particle transport in a channel flow with porous walls	Herterich Griffiths Field Vella
13/19	On a poroviscoelastic model for cell crawling	Kimpton Whiteley Waters Oliver
13/20	Complexity Plots	Thiyagalingam Walton Duffy Trefethen Chen
13/21	Glyph-based video visualization for semen analysis	Duffy Thiyagalingam Walton Smith Trefethen Kirkman-Brown Gaffney Chen

13/27	A well-posedness framework for inpainting based on coherence transport	März
13/28	Minimizing synchronizations in sparse iterative solvers for distributed supercomputers	Zhu Gu Liu
13/29	Computational probabilistic quantification of pro-arrhythmic risk from scar and left-to-right heterogeneity in the human ventricles	Wallman Bueno-Orovio Rodriguez
13/30	Population of human ventricular cell models calibrated with in vivo measurements unravels ionic mechanisms of cardiac alternans	Zhou Bueno-Orovio Orini Hanson Haywood Taggart Lambiase Burrage Rodriguez
13/31	On the eigenvalues and eigenvectors of nonsymmetric saddle point matrices preconditioned by block triangular matrices	Pestana
13/32	Singular inextensible limit in the vibrations of post-buckled rods: analytical derivation and role of boundary conditions	Neukirch Goriely Thomas
13/33	Interfacial deflection and jetting of a paramagnetic particle-laden fluid: theory and experiment	Tsai Griffiths Li Kim Stone
13/34	A lattice Boltzmann model for natural convection in cavities	Allen Reis

Copies of these, and any other OCCAM reports can be obtained from:

Oxford Centre for Collaborative Applied Mathematics
Mathematical Institute
24 - 29 St Giles'
Oxford
OX1 3LB
England
www.maths.ox.ac.uk/occam